Metal Patterning by Electrodeposition Assisted X-ray Lithography

John P. Katsoudas[1]*
Elena V. Timofeeva[2]*
Carlo U. Segre[1]

[1] Physics Department and Center for Synchrotron Radiation Research and Instrumentation, Illinois Institute of Technology, Chicago, IL 60616, USA
[2] Energy Systems Division, Argonne National Laboratory, Argonne, IL 60439, USA

*e-mail: katsjoh@iit.edu, etimofeeva@anl.gov

MAY 2011

The submitted manuscript has been created by Argonne National Laboratory, a U.S. Department of Energy laboratory managed by UChicago Argonne, LLC, under Contract No. DE-AC02-06CH11357 with the U.S. Department of Energy. The U.S. Government retains for itself, and others acting on its behalf, a paid-up, nonexclusive, irrevocable worldwide license in said article to reproduce, prepare derivative works, distribute copies to the public, and perform publicly and display publicly, by or on behalf of the Government

To be submitted to JOURNAL OF THE ELECTROCHEMICAL SOCIETY

Metal Patterning by Electrodeposition Assisted X-ray Lithography

John P. Katsoudas[1]*, Elena V. Timofeeva[2]*, Carlo U. Segre[1]

[1] Physics Department and Center for Synchrotron Radiation Research and Instrumentation, Illinois Institute of Technology, Chicago, IL 60616, USA
[2] Energy Systems Division, Argonne National Laboratory, Argonne, IL 60439, USA
*e-mail: katsjoh@iit.edu, etimofeeva@anl.gov

Abstract

Electrodeposition Assisted X-ray Lithography (EAXL) is a novel technique which can be an alternative to the LIGA process (X-ray lithography or *Lithographie, Galvanoformung,* and *Abformung*) for fabricating high aspect ratio structures. The approach forgoes four steps of a typical LIGA process (exposure of a photo resist to a masked x-ray beam, development-processing of the resist, electroplating into resist template and mold stripping) and is based on simultaneously exposing the substrate to masked x-rays within an electric field in a metal salt solution. This paper presents an overview of the current state of progress for this technique, and demonstrates the effect of the x-ray energy spectrum, the electrode overpotential and the electrode surface treatment on the morphology of patterned silver deposits. The results indicate that both the exposure to x-rays and an overpotential are necessary for formation and proper growth of the desired pattern while providing direction for further development of the technique.

Keywords: x-ray lithography, pattern formation, LIGA, electrodeposition, polyoxometallate, EAXL

1. Introduction

Patterned deposits have become important for many electronic, photonic, magnetic, ionic devices. The tools for patterned deposition are rapidly emerging offering a wide variety of techniques. Most of them can be categorized as direct-writing techniques that require no mask, soft lithography that relies on molecular self-assembly or use of pre-patterned substrates, and

masking techniques that use a pre-fabricated mask and a source of UV/visible light or x-rays to form the pattern. Direct writing techniques (scanning beam and scanning probe systems) exhibit the flexibility in pattern configuration, but are very slow, have limited manufacturing throughput and extremely high production costs due to point-by-point fabrication. Soft lithography is less expensive, however it has limited resolution and aspect ratio capabilities. Masking techniques generally provide lower fabrication costs, but due to diffraction and scattering of the beam some limitations in pattern resolution and aspect ratio also apply depending on the exposure source. LIGA has been recognized and developed as a unique technique for manufacturing microscopic structures with high aspect ratios [1] - critical requirements for microsystem applications. In a typical LIGA process, a thick polymer photo resist (PMMA or EPON SU-8) is exposed to a masked x-ray beam to translate the pattern from the prefabricated mask (deep x-ray lithography or DXRL step). The developed-processed resist with high aspect ratio extruded patterns is then used as an electroplating template. After overplating, a mold is stripped from the polymer substrate, and employed in a mass production scheme. The precision, spatial resolution, high aspect ratio and low sidewall roughness are the great advantages in LIGA processing; however this is still a niche technology with a rather limited spectrum of commercial applications. Being a multistep sequential process LIGA relies on many process variables, and its ability to produce consistently acceptable structures is proportional to the amount of time and effort invested at each of the manufacturing steps. The physical exposure time for DXRL structure typically requires between 4 and 8 hours (PMMA) of synchrotron beam time. The user defined beam parameters and the penetration depths needed to manufacture a mold makes DXRL an extremely expensive proposition from a “cost of exposure time vs. production” point of view.

Minimization of as many processing steps as possible would make the LIGA process a much more efficient and cost effective manufacturing technique. The novel method presented in this work forgoes four traditional processing steps involved in fabricating metallic structures with LIGA, and provides the proof of principle for a single step patterning with x-ray lithography

from metal salt solution. The approach is based on exposure of the substrate to masked x-rays during potentiostatic metal deposition. Projection of an x-ray grating onto the substrate demonstrated direct patterning with metallic silver. The ability of synchrotron radiation to penetrate the metallic salt solution within the experimental cell, while maintaining a high degree of collimation allows for fast production of patterned deposits in the wide x-ray beam (~10 cm) from a bending magnet. The beam from any other exposure source (ultraviolet or soft x-ray) would either dissipate before patterning occurred, or could not be masked (γ-rays).

2. Materials and Methods

The EAXL cell (Fig. 1a), which was specifically designed for this experiment, consisted of two graphite plates sandwiched between three 25 mm thick Teflon plates (ASTMD 1710), each Teflon plate having a 75 mm circular window bored out to allow the incident x-ray beam to pass. The graphite plates (Goodfellow, 319-120-39) served as x-ray bulkhead windows for the cell, and as the working and counter electrodes of the three-electrode system with the working electrode always being the downstream face. A silver-silver chloride (Ag/AgCl) electrode (BAS, MF-2052) was immersed into the cell from an orifice located at the top of the cell and used as a reference electrode. All the potentials reported in this paper are versus the potential of Ag/AgCl reference electrode. An electrolyte solution (0.1 M $AgNO_3$ in DI water) was injected into the cell from the bottom, removed from the top, and circulated in a closed loop by a peristaltic pump (Masterflex, L/S by Cole-Palmer). The flow rate of solution was maintained between 100-300 ml/min. Electrodeposition was conducted in a potentiostatic regime at low current densities/overpotentials in order to provide a homogeneous growth of the deposits. An EZstat potentiostat/galvanostat (NuVant Systems Inc., IN) was used in all the experiments. The optical microscopy images were acquired using Olympus BH2 and SteREO Discovery V.20 by Carl ZEISS.

The lithography mask was attached to the upstream face of the experimental cell (Fig. 1a), and the entire assembly was scanned through the incident x-ray beam using an Aerotech UNIDEX 500 lithography scanner (machine resolution .0001 mm) (Fig. 1b). The cell was scanned through the x-ray beam (size vert. 2mm x hor. 62mm) so as to avoid contact with the Teflon, and the scan rates ranged from 3.4 to 20 mm/sec.

The spectrum of the x-ray beam was altered during the experiment by reflection from a 879.50 mm long Pt coated mirror (Fig. 1b), essentially a low-pass filter whose cutoff energy is determined by the angle between the incident beam and the mirror. The x-ray spectrum for a given mirror angle was calculated using the modeling programs (XOP 2.11 [2] and Hephaestus [3]) and accounted for all components of the cell which were in line with the synchrotron beam as well as the position of the cell with respect to the beam source. Three different mirror angles were chosen for empirical comparison.

The three electrode cell was tested in the cyclic voltammetry (CV) regime prior to exposure to x-rays. The cathodic potential window was expanded from an open circuit potential (OCP, 0.43V vs. Ag/AgCl) by 50 mV steps (Fig. 2). The Nernst equilibrium potential (E_0) for silver deposition in 0.1 M $AgNO_3$ solution ($Ag^+ + e^- \Rightarrow Ag^0$) is at ~0.5V vs. Ag/AgCl, however one can see from the CVs in figure 2 that the onset of Ag phase formation is observed at potentials below 0.43V. To achieve noticeable deposition rates, while keeping nucleation rates under control, an electrodeposition potential of 0.35V vs. Ag/AgCl corresponding to -0.3 mA/cm^2 current density was used for the majority of the EAXL exposures (EAXL potential), but higher overpotentials were tested as well.

During exposures of $AgNO_3$ solutions to x-rays a side process of radiolysis was observed: unsupported silver nanoparticles were formed in the solution, due to simple one electron reduction of the silver ions. Both unsupported nanoparticles and deposits at the electrode were confirmed to be metallic silver by x-ray absorption spectroscopy.

3. Results and Discussion

3.1. The Approach

Irradiation of aqueous solutions leads to the radiolysis of water resulting in the formation of radicals, among which solvated electrons (e^-_{aq}) are strong reducing agents for the metal ions.[4] Their induced reduction of metal ions leads to the formation of atoms and metallic clusters. This technique has been successfully used in micro- and nano- fabrication either with a γ-ray source,[5,6] laser or electron beam [7] or more recently with x-rays.[8-10] Our approach to forming a metallic object of controlled size and shape relies on the combination of the radiolytic reduction of metal ions with the controlled potentiostatic deposition of metal from the solution.

The electrodeposition process promotes nucleation and growth of crystals at the electrode surface under the influence of an electric field. Competition between growth and nucleation determines the granularity, structure, and properties of the metallic deposits.[11] At low overpotentials the deposition rate is just slightly higher than the metal dissolution rate. The hypothesis tested in our series of experiments is that simultaneous exposure to the masked x-ray beam and low electrochemical overpotential induces patterned nucleation sites through the radiolysis mechanism,[8] while controlled electrochemical growth forms those nuclei into a continuous metal pattern at the electrode. This technique allows metal deposition only in the areas exposed to x-rays, while minimizing random nucleation outside the projected x-rays.

3.2. The Importance of the X-ray Spectrum

By adjusting the platinum-coated mirror angle one can alter the energy spectrum of x-rays incident on the electrochemical cell. The energy spectrum at the downstream electrode was calculated for three mirror angles, 6.00, 3.00 and 2.25 mrad, starting with the x-ray energy spectrum after reflection from the Pt mirror and the energy mass absorption by the front electrode and electrolyte (Fig. 3a). The solution concentration and the cell thickness determined

the overall amount of silver and water that interacted with the beam. The resultant energy spectra at the surface of the downstream electrode (Fig. 3b) show significant variations as a function of the mirror angle. At 6.00 mrad the photon flux is an order of magnitude less that at 3.00 and 2.25 mrad with maximum intensity at 12 keV. At a mirror angle of 3.00 mrad the maximum intensity is observed at 25 keV and begins to roll off above the peak. At 2.25 mRad the intensity peak is at 25 keV as well, however the energy roll off is more gradual and only at 44 keV does it decrease by one order of magnitude, allowing for significant flux of higher energy photons to the working electrode. In order to select the best energy spectrum for the EAXL experiments, each of these mirror angles was used to expose a silica gel matrix placed at the working electrode and impregnated with $AgNO_3$ solution. The silica gel served to immobilize the metal nanoparticles formed by radiolysis and therefore, to capture a three-dimensional pattern of the mask formed during exposures. The effects of different mirror angles are clearly seen at inserts to figure 3b. At a mirror angle of 6.00 mrad non-continuous patterns comprised of individual metal clusters are formed in the gel, with intensity weakening toward the downstream electrode. The clear gel color indicates an insignificant amount of Ag nanoparticles formed through radiolysis outside the beam boundaries. Random nucleation is observed at the electrode surface. At 3.00 mrad one can see a significant increase in the density of metal patterns penetrating all the way through the gel along with a change in the gel color due to the formation of unsupported Ag nanoparticles outside the patterned area. Again, in this case, no pattern is formed at the downstream electrode. A significantly different result is obtained at a mirror angle of 2.25 mrad: the patterns are continuous metallic silver formed all the way through the gel to the downstream electrode surface. The dark color of the gel indicates high rates of nanoparticle formation through the reduction of metal ions by diffusing radiolysis activated species. Since the additional absorption by the silica gel is negligible and patterning at the downstream electrode occurred only at 2.25 mrad it was concluded that high energy x-rays are necessary to observe a significant effect on electrodeposition at the downstream electrode. All EAXL exposures discussed below were performed with the mirror angle at 2.25 mrad.

3.3. The Mechanism of Pattern Formation

The mechanism of pattern formation was investigated by performing a two-step exposure. The electrode was divided into three zones (A, B and C). First, zones A and B were exposed for 1 hour to masked x-rays at an open circuit potential (OCP, i.e. without any control of the electrode potential). After the OCP exposure, the electrolyte solution was replaced with a fresh AgNO3 solution, and a EAXL potential of 0.35V vs. Ag/AgCl was applied to the working electrode during x-ray exposure of zones B and C. Thus, the middle zone (B) was exposed to x-rays during both the 1st and 2nd exposure steps. Figure 4 illustrates the morphology of deposits obtained in these three zones.

Zone A (Fig. 4a) was exposed to masked x-rays for 1 hour during the first step and only to the electric field during the 2nd hour, and showed no pattern formation. Random nucleation with quite dense and rather small crystallites was observed. Zone B (Fig. 4b), was exposed to patterned x-rays for 1 hour and simultaneously to x-rays and the electric field during the second step. It has quite large, discontinuous crystallites that formed mostly in the spots exposed to x-rays with some surrounding random nucleation. Zone C (Fig. 4c) was only exposed to x-rays and an electric field for 1 hour simultaneously. A continuous pattern of silver crystals formed where the x-rays illuminated the electrode, very few random nuclei formed outside the pattern.

This two-step exposure demonstrates that nucleation is a critical part of the pattern formation and only with simultaneous exposure to x-rays and overpotential are the correct conditions for the formation of continuous patterns achieved. X-rays at OCP do not provide adhesive nucleation directly at the surface, rather they activate the solution through radiolysis and the activated species diffuse, and nucleate randomly at the electrode surface or aggregate into unsupported nanoparticles.

It is well known that nucleation is a critical step in electrochemical phase growth. The probability of spontaneous nucleation is affected by the nature of the substrate, deposit/substrate binding energy, crystallographic misfit, applied overpotential, and the concentration of metal ions in the solution. At low overpotentials nucleation rates are low and a linear growth of existing nuclei occurs. Electrodeposition in zone A (Fig. 4a), conducted without x-ray exposure, resulted in the growth of all preexisting nucleated sites which formed during the x-ray exposure at OCP (first step). Zone B (Fig. 4b) also had random nuclei formed, during the first exposure step, however electrodeposition was assisted by the masked x-rays and the crystal growth favored the nuclei located in the path of the beam. The larger grain size observed in zone B suggests that no new nucleation occurred during the 2nd step in zone B due to low overpotentials and predominant growth of existing nuclei. Electrodeposition in zone C (Fig. 4c) started simultaneously with exposure to masked x-rays directed at an unaltered electrode surface. Nucleation and growth occurred continuously in the beam path with minor random nucleation, which probably could be avoided in the future by simply adjusting the value of overpotential and/or solution concentration. The results of this two-step exposure also suggest that x-rays could be used to guide patterned nucleation at the electrode surface during potentiostatic electrodeposition.

The morphologies of the deposits formed in zone C (Fig. 5a and c) and electrodeposits formed at the same electrode outside the masked x-ray path (Fig. 5b) also show significant differences. The nuclei formed in areas exposed to x-rays during electrodeposition have an average crystallite size of < 20 μm (Fig. 5a) while the crystallites formed in the area distanced from the beam path (Fig. 5b) are significantly larger (~ 60 μm). The density of nucleation is an order of magnitude higher in areas of the electrode exposed to x-rays. Despite the large size of the mask features a sharp boundary is observed at the edge of x-ray beam pattern (Fig. 5c) demonstrating that nucleation is favored in areas exposed to x-rays and once the number of

nucleation centers complies with the applied electrodeposition rate the metal growth continues on the existing centers.

The possible reasons for such dramatic effects of x-rays on the electrodeposition process include: (a) the presence of radiolysis-activated species; (b) local modification of the surface potential by the x-ray beam; (c) temperature gradients at the surface exposed to the masked x-rays; or some combination thereof. Since it was shown that high-energy photons are required at the electrode surface for pattern formation, we suggest the radiolysis-activated species cannot be the sole reason for patterning and the other reasons are probably important.

3.4. The Effect of Overpotential.

The effects of the electrode overpotential on the deposit morphology were studied at a 1.5-hour deposition time, 0.1M $AgNO_3$ concentration, and a mirror angle of 2.25 mrad. A potential of 0.35 V vs. Ag/AgCl was applied to the working electrode, which is 0.15V negative of E_0 and 0.07 V negative of the onset of Ag deposition (Fig. 2), produced a continuous pattern composed of interconnected metal grains with very little deviation from the mask features (Fig. 6a). The shift of the electrode overpotential by 0.22 V negative of E_0 (0.28 V vs. Ag/AgCl) resulted in deposits with the onset of dendrite-like growth (Fig. 6b). At overpotential of 0.27 V negative to E_0 (0.23 V vs. Ag/AgCl) taller deposits with significant branching were formed in the beam path (Fig. 6c). The higher overpotential values corresponded to higher deposition currents resulting in a shift of the equilibrium between nucleation and growth created by the conditions of simultaneous exposure and produced dendrite-like deposits with lower pattern resolution and poor homogeneity.

3.5. The Effect of Surface Treatment

The success of the patterning process depends on the x-ray spectrum, electrode overpotential, and deposition time. To further investigate the mechanism of pattern formation half of the graphite electrode was treated with a solution of dodecatungstic acid ($H_3PW_{12}O_{40}$), which belongs to the class of polyoxometalates with Keggin structure.[12] These types of compounds are well known to be thermally stable and capable of reversible red/ox reaction, and photoreduction upon exposure to UV light in the presence of electron donors.[13] Polyoxoanions also specifically adsorb on various surfaces, including graphite,[14] allowing for an easy surface treatment: immersing half of the electrode plate into 10^{-3} M solution for a half-hour and rinsing off excess solution with de-ionized water.

The pattern formed on the half of the electrode treated with PW_{12} is more precise, and rather tall (Fig. 7a), while the untreated surface resulted in a wider pattern composed of many smaller crystals and significant number of random nuclei outside the masked x-ray pattern (Fig. 7b). The role of $H_3PW_{12}O_{40}$ species in pattern formation is most likely serving as a reducing buffer that accumulates radiolysis-activated electrons and promotes the reduction of silver ions within the masked beam. At the given metal ion concentration the presence of such species at the electrode should favor the growth of a metal particle rather than a nucleation of new centers as observed in the experiment.

3.6. Feature Resolution

Aspect ratio and resolution are important figures of merit for any lithographic technique. There is little to no limitation related to the resolving power of x-rays. Since their wavelength is on the order of the atomic scale, limiting issues of traditional ultraviolet and visible light lithography, such as diffraction and focusing, do not apply to x-ray lithography. Therefore, the resolvable feature sizes in x-ray lithography are only limited by the available masking technologies for high energy x-rays. The patterns obtained so far with single step x-ray

lithography are polycrystalline, comprised of interconnected continuous crystalline grains. Figures 8a and 8b compare the Au/silicon lithography mask to the Ag deposit on the graphite electrode obtained with the mask. The width of deposits is very close to the mask feature sizes of with less than 20% deviations that are due to non-selective 3D growth of sites nucleated within the projected x-ray pattern. Use of a mask with finer features at the same EAXL conditions (0.35V and 2.25 mrad mirror angle) allowed for the formation of smaller patterns (Fig. 8c) at the same deposition conditions and surface roughness of the substrate. Therefore, the feature size of the deposit is mostly defined by the mask resolution.

High roughness of the electrode surface indicates a wide range of surface energies - a potential obstacle towards obtaining homogeneous nucleation throughout the pattern. Use of a more homogeneous electrode surface is likely to improve the quality and aspect ratio of deposits. Another avenue for improving the aspect ratio of deposits is to create conditions for selective growth in one crystal plane. Further work in this direction will allow this technique to establish itself as a potential candidate for micro- and nanomanufacturing.

4. Conclusions

This paper investigates the mechanism and factors contributing to the formation of the patterned metal deposits during the simultaneous exposure to masked x-rays and electric field. This new approach to x-ray lithography eliminates the use of any resist-substrate material. A simultaneous application of masked x-rays and electrode overpotential is critical for patterning and penetration of higher energy photons to the electrode surface is required in order to form patterned electrodeposits. The patterned silver deposits are continuous structures comprised of interconnected crystallites. Nucleation centers form within the x-ray beam, however their non-selective three-dimensional growth results in ~20% deviation from the mask features and nearly 1:1 aspect ratio of the deposits. The effects of the overpotential and electrode surface treatments illuminate the possible mechanisms behind patterning. The nucleation is suggested as a critical

step in patterning, while the electrodeposition rates are critical for the homogeneity of the deposits. The avenues for further development of the technique are using a more homogeneous electrode surface and controlling the selective growth in one crystal plane.

5. Acknowledgements

We thank Ralu Divan for her guidance and help, Jeremy Kropf for his critical opinion on design and the concept of the experiments, Jules Routbort for enthusiastic support of the project, and NuVant Inc. for providing us with equipment for electrochemical part of experiment. MRCAT operations are supported by the Department of Energy and the MRCAT member institutions. Use of the Argonne National Laboratory and Advanced Photon Source is supported by the U.S. Department of Energy, Office of Science, Office of Basic Energy Sciences, under Contract No. DE-AC02-06CH11357.

6. References

1. V. Saile, U. Wallrabe, O. Tabata, J.G. Korvink, *LIGA and Its Applications*; Wiley-VCH, Weinheim, Germany (2009).

2. M.S. del Rio, R.J. Dejus, *Advances in Computational Methods for X-Ray and Neutron Optics*, **5536**, 171 (2004).

3. B. Ravel, M. Newville, *Journal of Synchrotron Radiation*, **12**, 537 (2005).

4. G.V. Buxton, R.M. Sellers, *Coordination Chemistry Reviews*, **22**, 195 (1977).

5. D.B. Yu, X.Q. Sun, J.T. Bian, Z.C. Tong, Y.T. Qian, Physica *E-Low-Dimensional Systems & Nanostructures*, **23**, 50 (2004).

6. H. Remita, I. Lampre, M. Mostafavi, E. Balanzat, S. Bouffard, *Radiation Physics and Chemistry*, **72**, 575 (2005).

7. F. Stellacci, C.A. Bauer, T. Meyer-Friedrichsen, W. Wenseleers, V. Alain, S.M. Kuebler, S.J.K. Pond, Y.D. Zhang, S.R. Marder, J.W. Perry, *Advanced Materials*, **14**, 194 (2002).

8. R. Divan, D.C. Mancini, N. Moldovan, L. Assoufid, Y.S. Chu, Q. Ma, R.A. Rosenberg, 2003 *International Semiconductor Conference*, **1-2**, 39 (2003).

9. Q. Ma, R. Divan, D.C. Mancini, R.A. Rosenberg, J.P. Quintana, D.T. Keane, *Applied Physics Letters*, **89**, 83114 (2006).

10. M.F. Bertino, R.R. Gadipalli, L.A. Martin, L.E. Rich, A. Yamilov, B.R. Heckman, N. Leventis, S. Guha, J. Katsoudas, R. Divan, D.C. Mancini, *Nanotechnology*, **18**, 315603 (2007).

11. E. Budevski, G. Staikov, W.J. Lorenz, *Electrochemical Phase Formation and Growth: An introduction to the Initial Stages of Metal Deposition*, VCH Verlagsgesellschaft mbH, Weinheim, Germany (1996).

12. M.T. Pope, Y. Jeannin, M. Fournier, *Heteropoly and isopoly oxometalates,* Springer-Verlag, Berlin (1983).

13. T. Yamase, *Chemical Reviews*, **98**, 307 (1998).

14. W.G. Klemperer, C.G. Wall, *Chemical Reviews*, **98**, 297 (1998).

Figure Captions:

Figure 1. (a) Experimental cell for simultaneous exposure to X-rays and electric field: R.E. – Ag/AgCl reference electrode; W.E. – working electrode; C.E. – counter electrode. (b) Schematic of MRCAT10BM beamline (APS), showing the position of lithography scanning stage and Pt coated mirror used in the experiment.

Figure 2. Cyclic voltammetry at a carbon graphite electrode in 0.1 M $AgNO_3$ solution; scan rate 10 mV/s; cathodic potential was expanded 50 mV per each cycle.

Figure 3. (a) Energy spectra of X-ray beam reflected from Pt mirror at various angles (left Y-axis) and the transmission coefficient through 0.1 M $AgNO_3$ in water at the given width of the cell (right Y-axis); (b) the characteristic energy spectrum reaching the working electrode (downstream plate) calculated for three different mirror angles with the inclusion of all absorbing media. Inserts on figure 3b illustrate the effects of one hour exposure to x-rays at various mirror angles on the cell environment, captured in a silica gel at the working electrode (back plate).

Figure 4. Set of micrographs showing two step exposure: (a) zone A, exposed to masked x-rays first (1hour), then electric field at 0.35 V for 1 hour (no x-rays); (b) zone B, exposed to masked x-rays first (1 hour), then x-rays + potential (1 hour); (c) zone C, simultaneously exposed to x-rays and potential (1 hour).

Figure 5. Morphology of electrodeposits resulted from: (a) 1 hour simultaneous exposure to x-rays at 0.35 V potential (zone C); (b) 1 hour electrodeposition at 0.35 V without exposure to x-rays; (c) boundary between exposed to x-rays (left) and masked (right) areas in zone C (1 hour of simultaneous x-ray exposure and electrodeposition at 0.35 V).

Figure 6. Morphologies of deposits formed at 2.25 mRad mirror angle and various electrodeposition potentials: (a) 0.350 V; (b) 0.280 V; (c) 0.230 V during 1.5 hour exposures.

Figure 7. Deposit morphologies formed during 1 hour at 0.35V, 2.25 mrad on (a) polyoxotungstate ($H_3PW_{12}O_{40}$) treated part of the electrode, and (b) untreated electrode area exposed to masked x-rays.

Figure 8. Comparison of the lithography mask features (Au on silicon) (a) to the size of Ag deposits on graphite (b) obtained with the mask; (c) a finer pattern of silver obtained using a mask with smaller size features. EAXL conditions 1 hour at 0.35V and 2.25 mrad mirror angle.

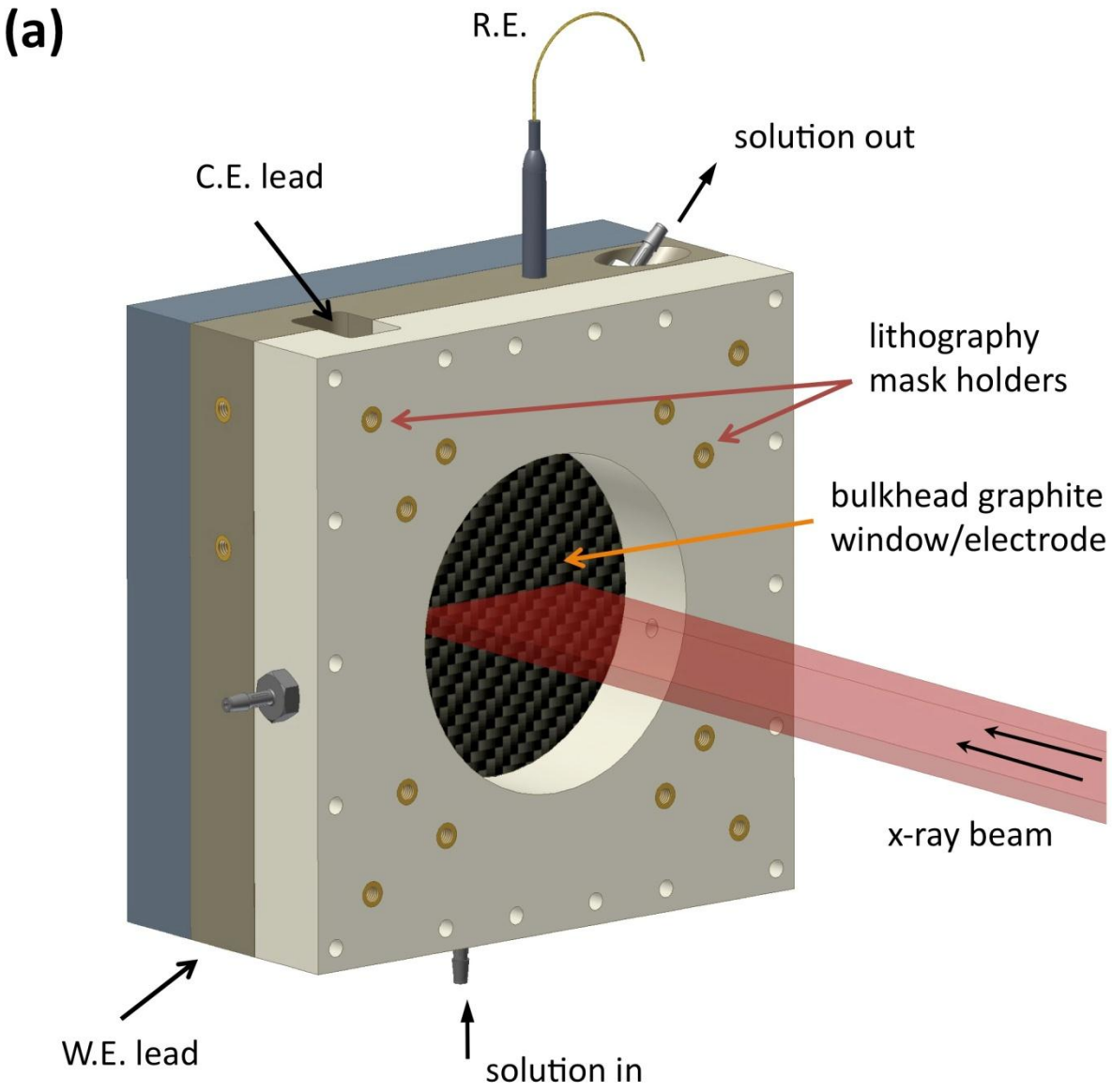
(a)
R.E.
solution out
C.E. lead
lithography
mask holders
bulkhead graphite
window/electrode
x-ray beam
W.E. lead
solution in

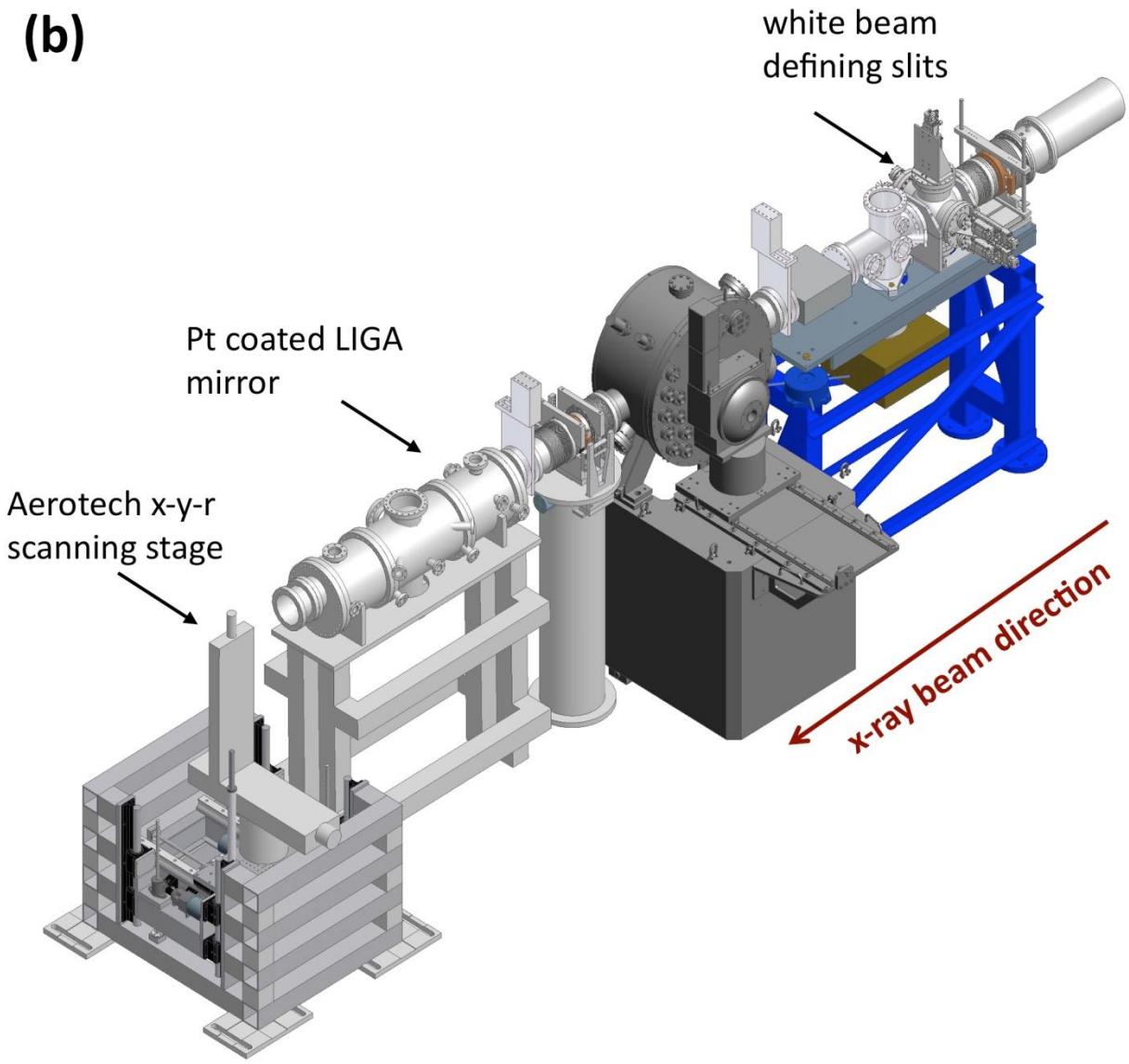

Figure 1. (a) Experimental cell for simultaneous exposure to X-rays and electric field: R.E. – Ag/AgCl reference electrode; W.E. – working electrode; C.E. – counter electrode. (b) Schematic of MRCAT10BM beamline (Advansed Photon Source, Argonne, IL), showing the position of lithography scanning stage and Pt coated mirror used in the experiment.

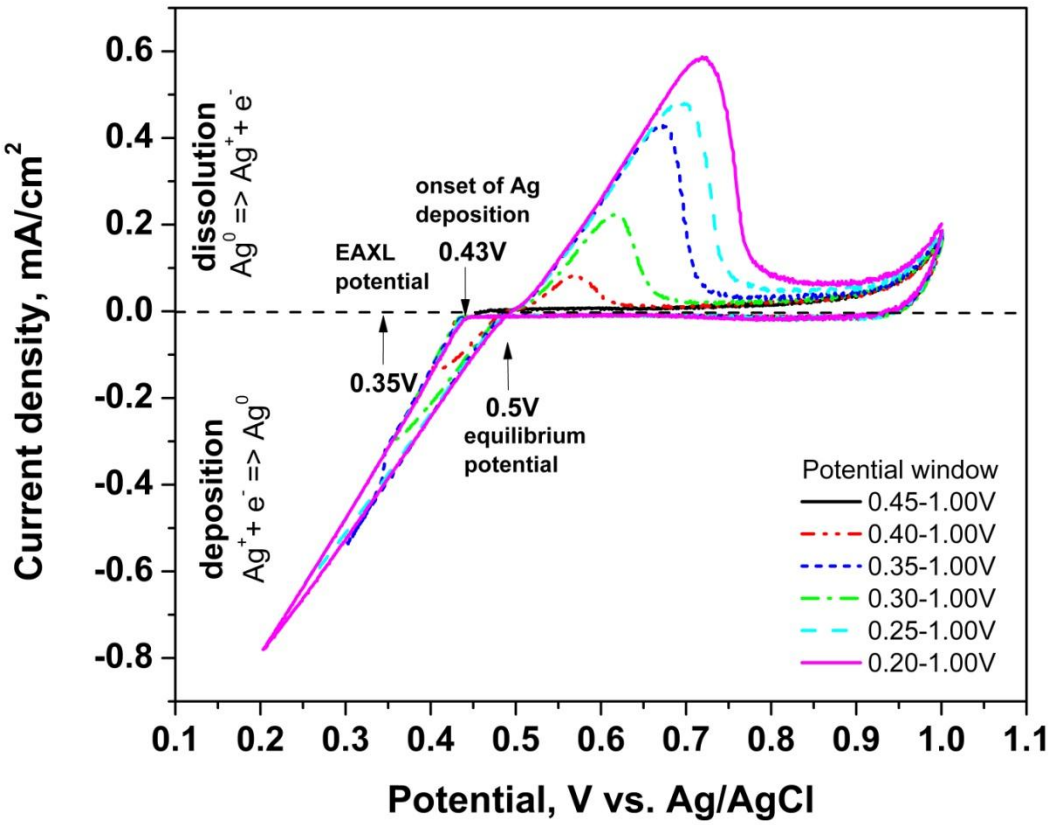

Figure 2. Cyclic voltammetry at a carbon graphite electrode in 0.1 M $AgNO_3$ solution; scan rate 10 mV/s; cathodic potential was expanded 50 mV per each cycle.

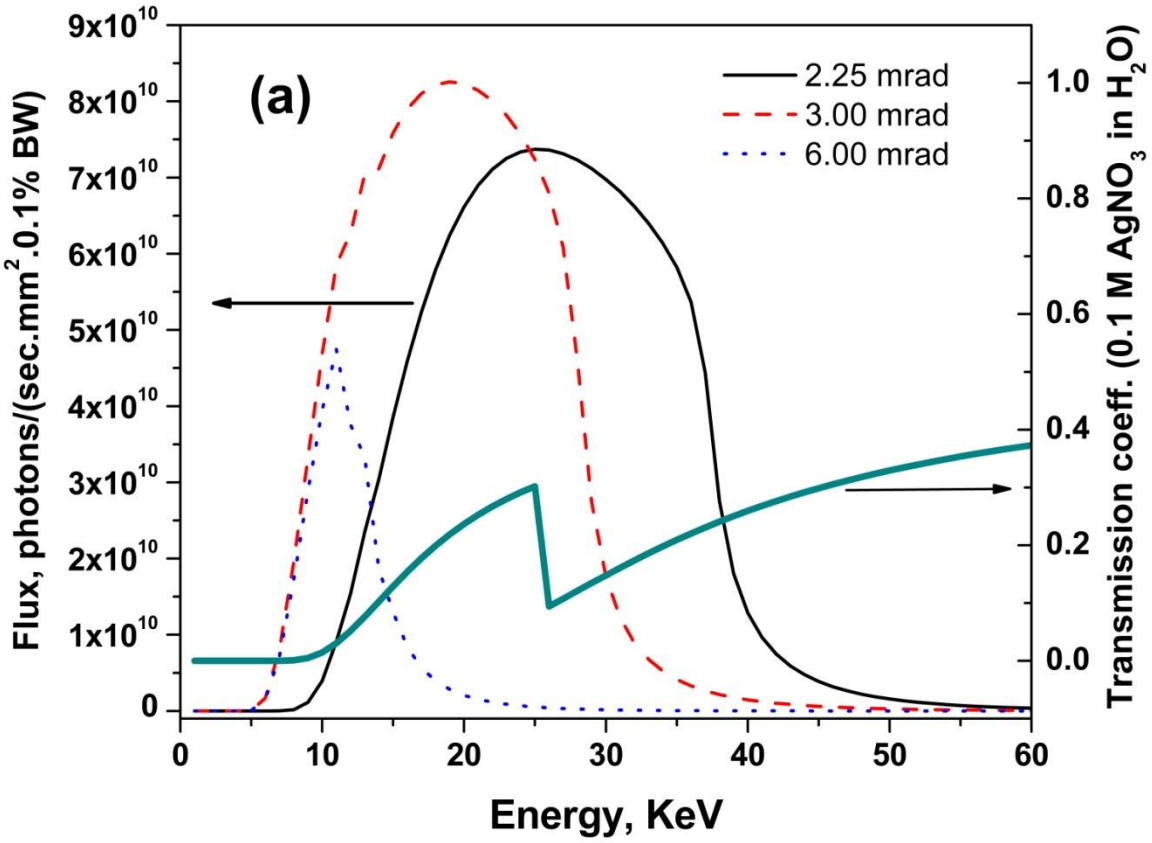
(a)
2.25 mrad
3.00 mrad
6.00 mrad
Flux, photons/(sec.mm^2.0.1% BW)
Transmission coeff. (0.1 M $AgNO_3$ in H_2O)
Energy, KeV
9x10^{10}
8x10^{10}
7x10^{10}
6x10^{10}
5x10^{10}
4x10^{10}
3x10^{10}
2x10^{10}
1x10^{10}
0
1.0
0.8
0.6
0.4
0.2
0.0
0
10
20
30
40
50
60

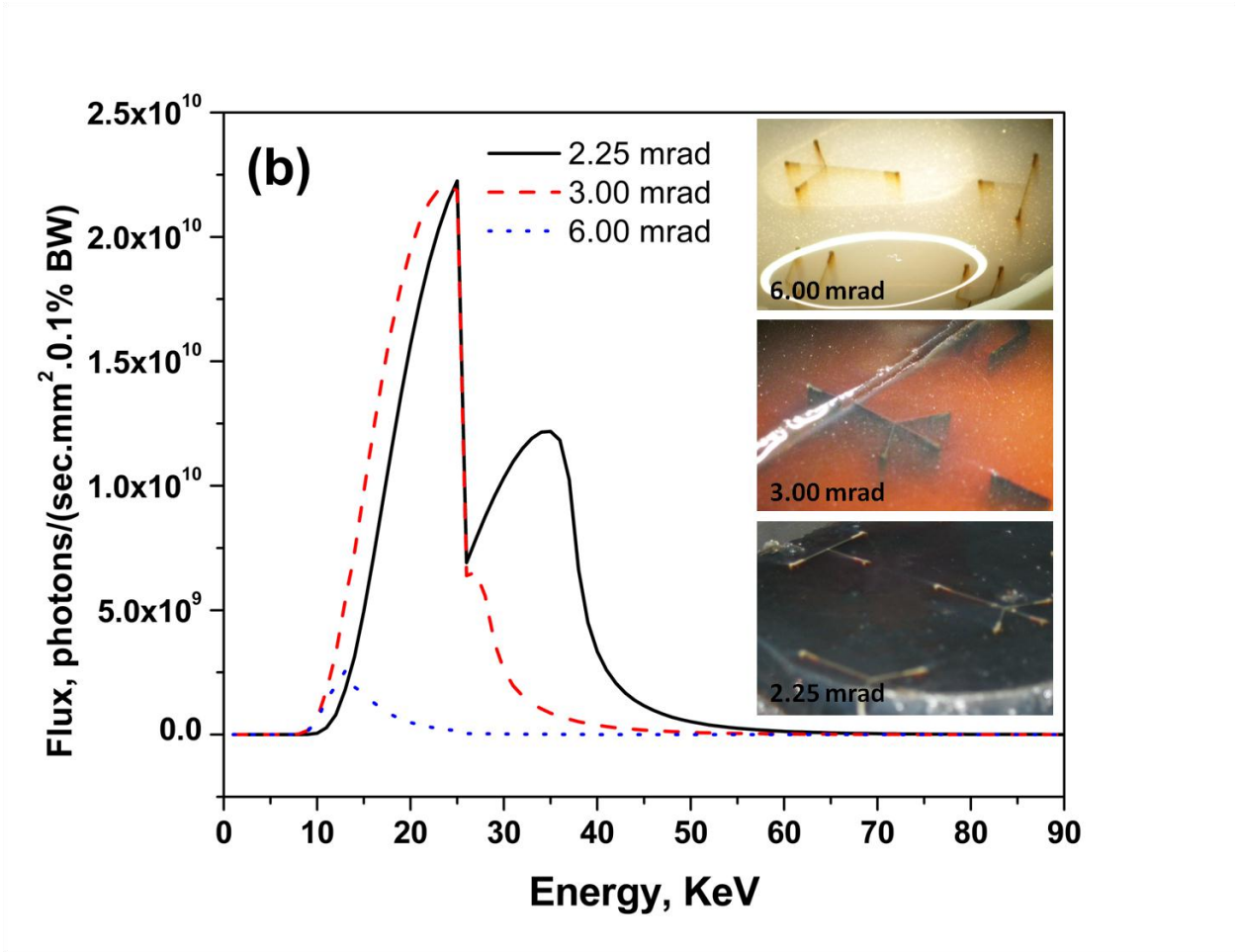

Figure 3. (a) Energy spectra of X-ray beam reflected from Pt mirror at various angles (left Y-axis) and the transmission coefficient through 0.1 M $AgNO_3$ in water at the given width of the cell (right Y-axis); (b) the characteristic energy spectrum reaching the working electrode (downstream plate) calculated for three different mirror angles with the inclusion of all absorbing media. Inserts on figure 3b illustrate the effects of one hour exposure to x-rays at various mirror angles on the cell environment, captured in a silica gel at the working electrode (back plate).

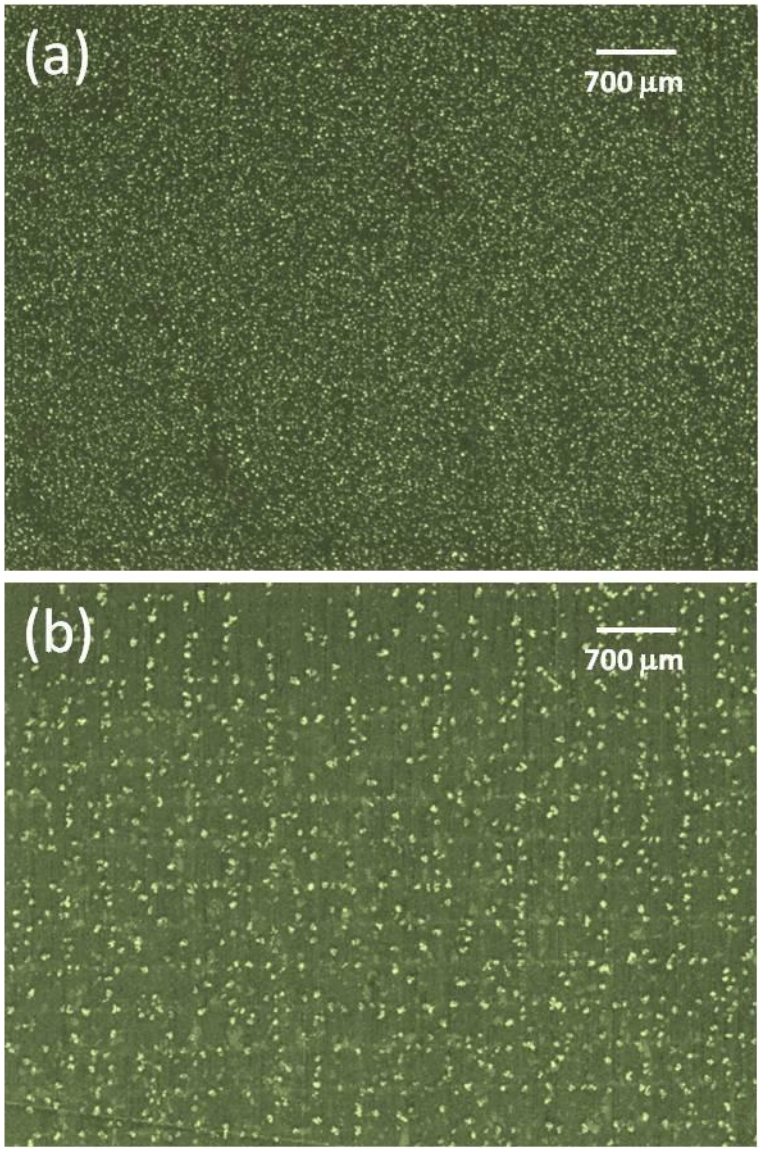
(a)
700 μm
(b)
700 μm

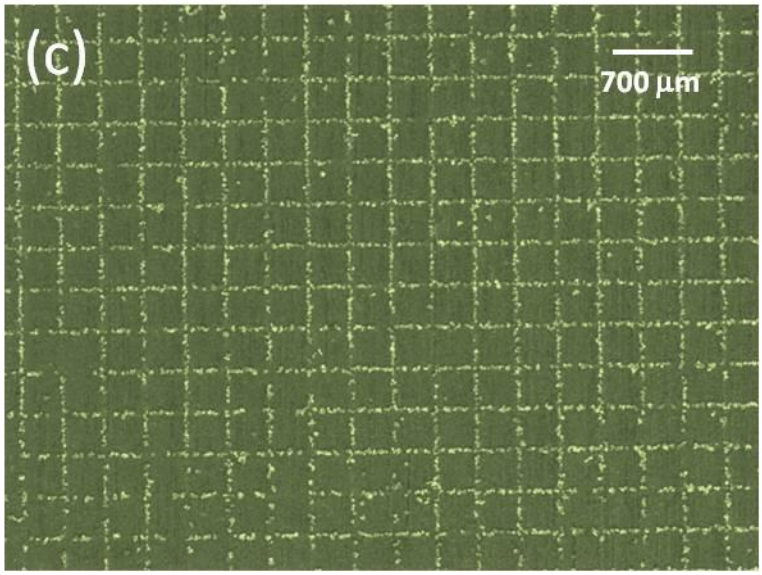

Figure 4. Set of micrographs showing two step exposure: (a) zone A, exposed to masked x-rays first (1hour), then electric field at 0.35 V for 1 hour (no x-rays); (b) zone B, exposed to masked x-rays first (1 hour), then x-rays + potential (1 hour); (c) zone C, simultaneously exposed to x-rays and potential (1 hour).

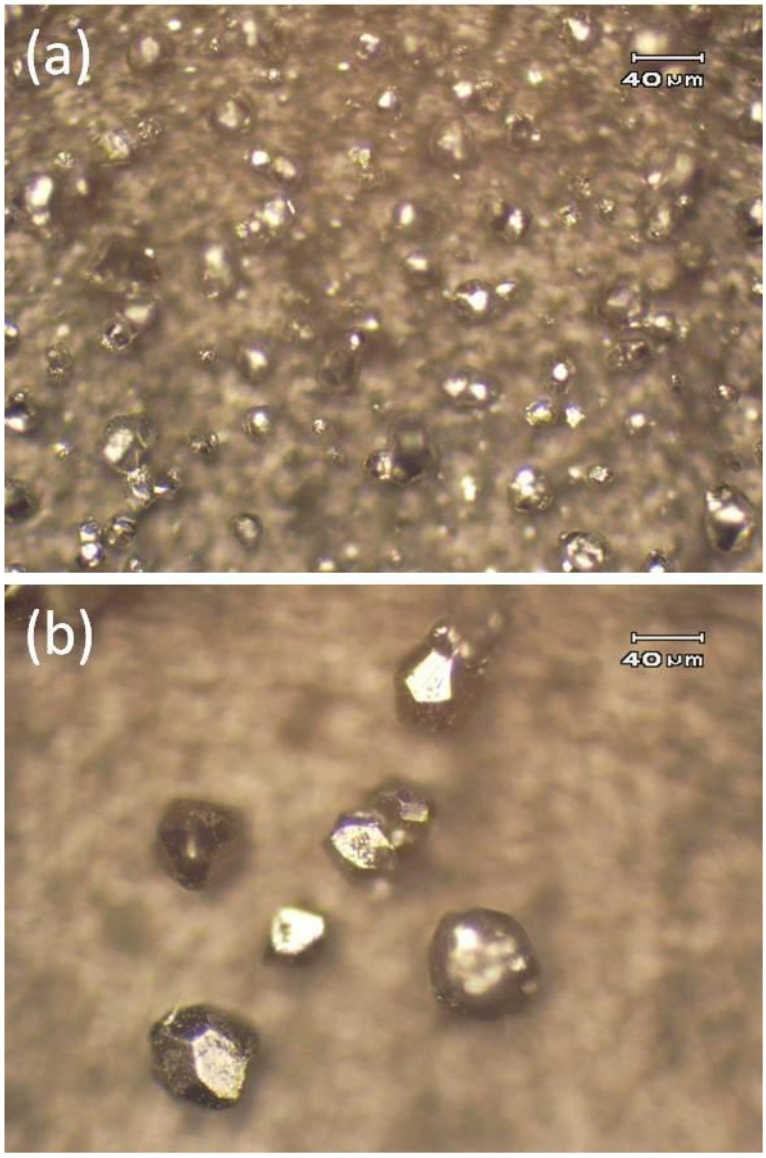
(a)
40 μm
(b)
40 μm

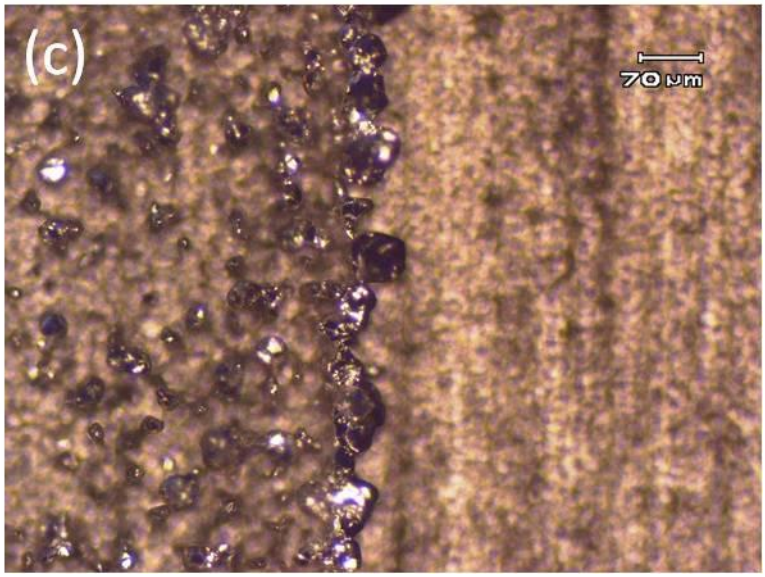

Figure 5. Morphology of electrodeposits resulted from: (a) 1 hour simultaneous exposure to x-rays at 0.35 V potential (zone C); (b) 1 hour electrodeposition at 0.35 V without exposure to x-rays; (c) boundary between exposed to x-rays (left) and masked (right) areas in zone C (1 hour of simultaneous x-ray exposure and electrodeposition at 0.35 V).

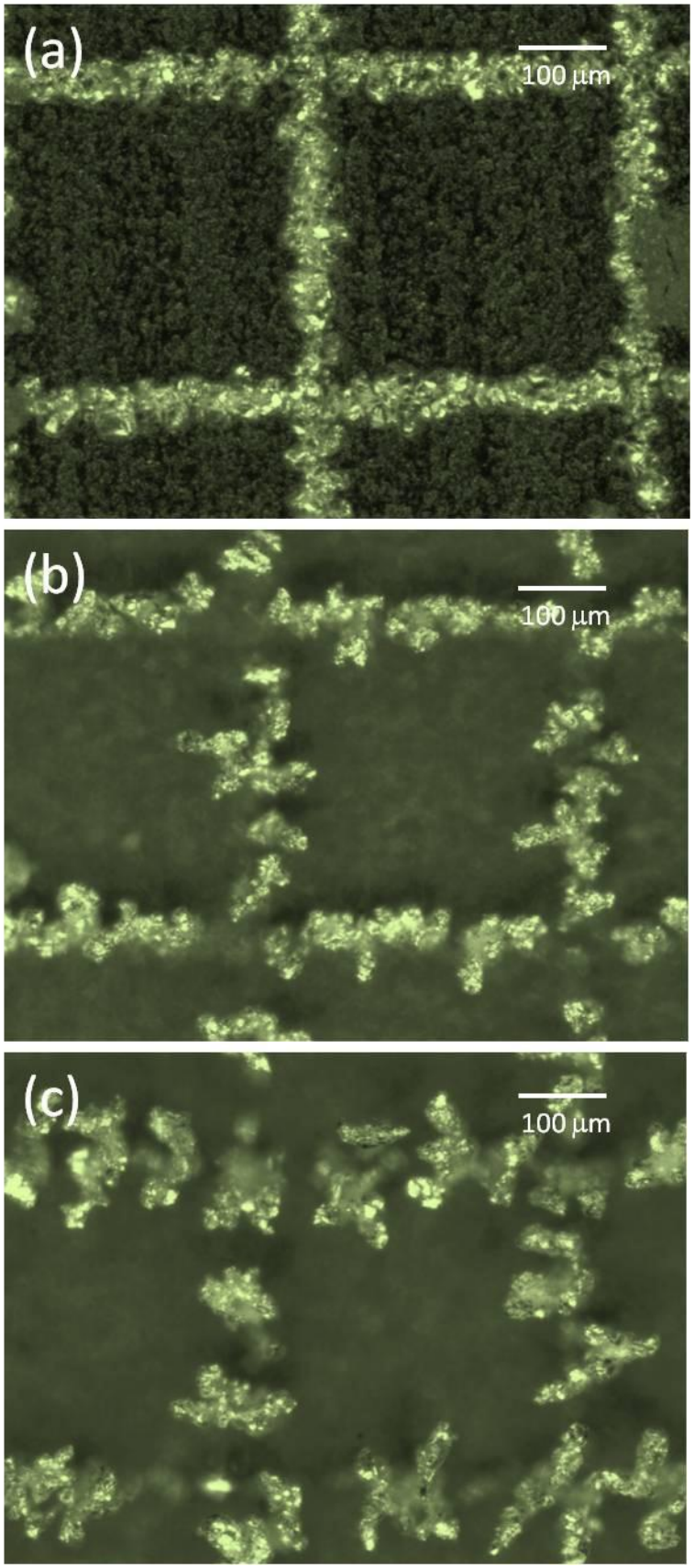
(a)
100 μm
(b)
100 μm
(c)
100 μm

Figure 6. Morphologies of deposits formed at 2.25 mRad mirror angle and various electrodeposition potentials: (a) 0.350 V; (b) 0.280 V; (c) 0.230 V during 1.5 hour exposures.

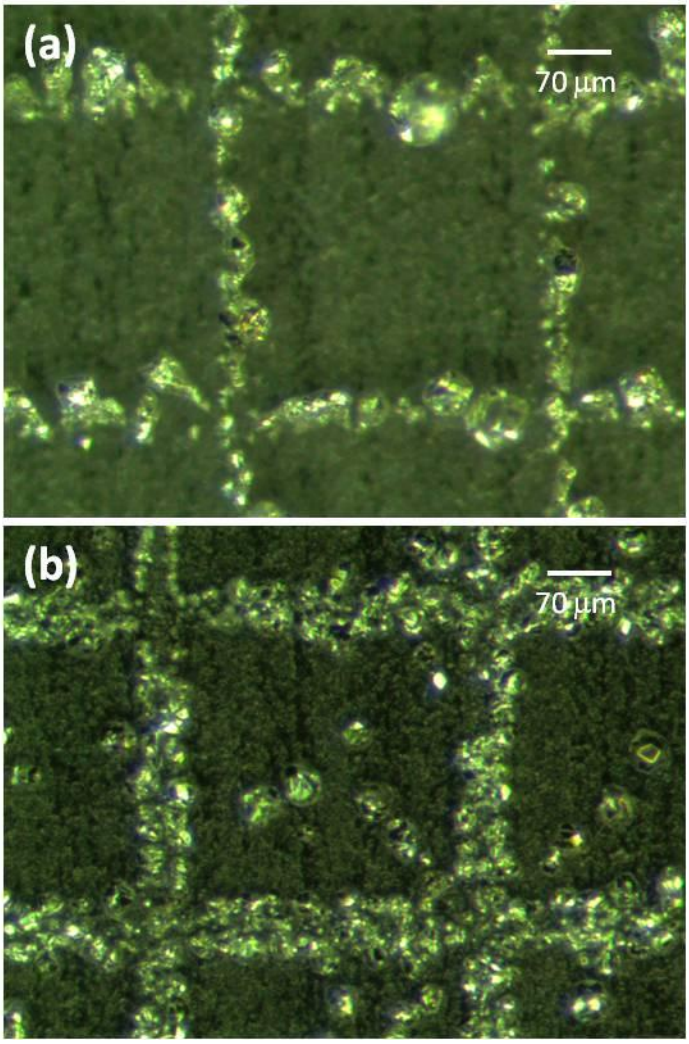

Figure 7. Deposit morphologies formed during 1 hour at 0.35V, 2.25 mrad on (a) polyoxotungstate ($H_3PW_{12}O_{40}$) treated part of the electrode, and (b) untreated electrode area exposed to masked x-rays.

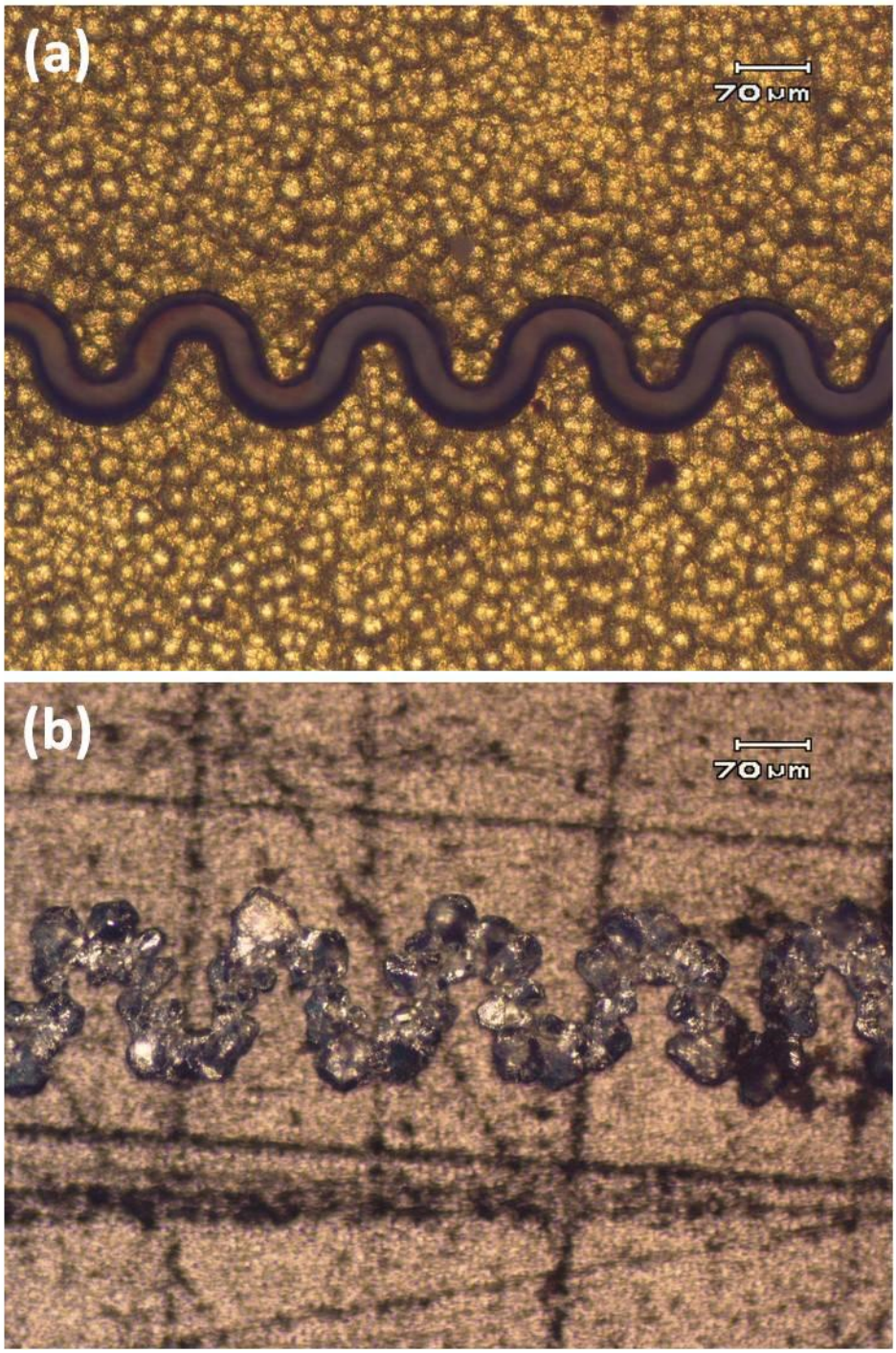
(a)
70 μm
(b)
70 μm

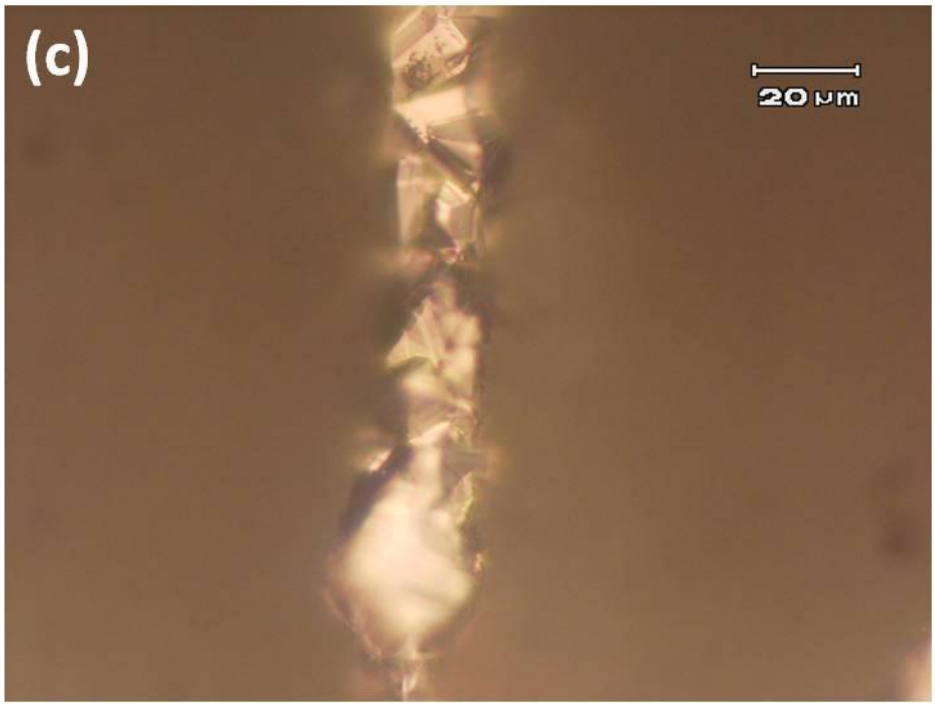

Figure 8. Comparison of the lithography mask features (Au on silicon) (a) to the size of Ag deposits on graphite (b) obtained with the mask; (c) a finer pattern of silver obtained using a mask with smaller size features. EAXL conditions 1 hour at 0.35V and 2.25 mrad mirror angle for both exposures.